DEVELOPMENT OF NAVIGATION ALGORITHMS FOR NAP-OF-THE-EARTH UAV FLIGHT IN A CONSTRAINED URBAN ENVIRONMENT

Murray Ireland, David Anderson
University of Glasgow
m.ireland.1@research.gla.ac.uk; Dave.Anderson@glasgow.ac.uk

Keywords: *MAV; quadrotor; inertial navigation; extended Kalman filter*

Abstract

Inertial measurement units (IMU) have a ubiquitous presence on unmanned aircraft, but are often used in combination with a number of additional sensors, including GPS. Small unmanned vehicles such as the micro air vehicle (MAV) often operate in urban or natural canyons, where GPS coverage is not guaranteed. In the absence of both GPS and any additional sensors, it is of interest to determine how long the MAV can continue to follow a pre-calculated flight path. In particular, the benefits of employing an accurate system model in a navigation solution are explored. The extended Kalman filter is the standard in navigation algorithms and is employed here, due to its ability to capture the non-linearities in aircraft dynamics.

Simulation testing is undertaken using the Qball-X4 quadrotor MAV as the source of the vehicle dynamics, parameters and sensor errors. The results of a strapdown inertial navigation system (SDINS) are compared to those of an INS augmented by a dynamic model of the quadrotor. Three iterations of the simulation are considered: one with no process or measurement noise; a second with measurement noise obtained from experimental tests and some process noise; and a final iteration including the vibration interference from the propellers, found to affect the inertial sensors of the Qball during flight.

While the use of a system model in the navigation algorithm is found to significantly improve the Kalman filter estimates of the simulated states, the effects of the propeller vibration negate its ability to do so to a level which has practical application. Future experimental testing requires that the vibration interference be removed or incorporated into the Kalman filter model.

1 Introduction

Micro Air Vehicles (MAV) are a relatively recent subset of the Unmanned Aerial Vehicle (UAV). The size and manoeuvrability of rotorcraft MAVs in particular makes them ideally suited to flight in such constrained environments as urban (or natural) canyons. These settings, however, can have an impact on the aircraft in other ways. The majority of aircraft use GNSS (global navigation satellite system), usually GPS, for position tracking, requiring line of sight with at least four satellites. While this is not an issue for aircraft which operate in open spaces, vehicles in urban canyons may be subject to frequent and extended loss of GNSS position feedback. Often the solution would be to avoid areas of satellite occlusion, but this may not always be an option for limited endurance aircraft like the MAV. Consider a potential mission for an MAV such as the quadrotor, where it is required to pass through a series of waypoints in an environment, by way of an optimal path [1] (Figure 1). This allows the aircraft to target any points of interest while maximising power efficiency and endurance. In following this path, the GNSS signal may be lost for an extended period of time. The choice between choosing this path or a longer, suboptimal one with better satellite coverage may not be a choice at all when the limited power systems of the quadrotor are considered. The goal is therefore to ensure the optimal path is followed as closely as possible, in the absence of GNSS or an alternative external source of feedback.

There a number of ways of obtaining position data without relying on external systems. These methods typically include the use of additional sensors such as laser rangefinders [2], sonar and cameras [3]. More advanced techniques may employed, such as simulta-
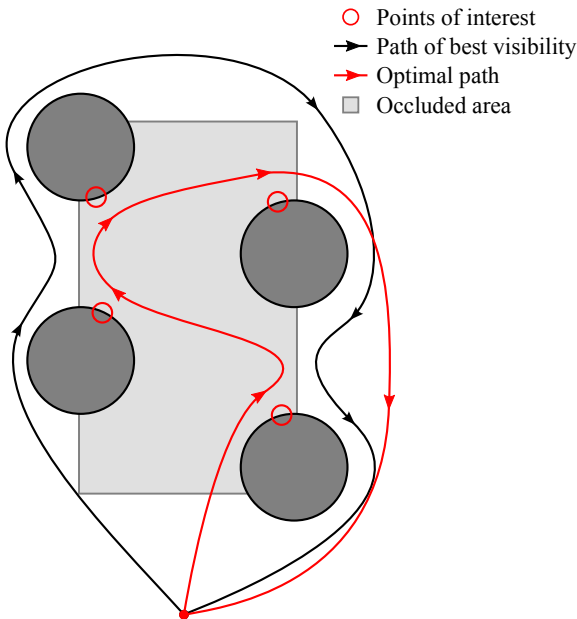
Fig. 1 Reliance on GPS limits the route an MAV can follow to exposed areas. This restricts the aircraft's ability to follow an optimal path.

Fig. 2 Qball-X4 quadrotor MAV.

neous localisation and mapping (SLAM), which uses the vehicle sensors to build a map of the environment [4]. However, additional sensors may be prohibitively expensive, heavy and/or bulky. Additionally, the extra power consumed by these sensors may also negate the benefits of pursuing an optimal flight path. Finally, the limited processing power of a typical MAV embedded computer limits the intensity of the operations it can perform. Considering a worst-case scenario, the quadrotor may be forced to rely on the most fundamental of sensor systems – the inertial measurement unit (IMU). A standard 9 degrees-of-freedom IMU carries accelerometers, gyroscopes and often magnetometers. Those found on MAVs are often of poor quality as a result of their size and design and carry a number of errors in their measurements. Integration of accelerometer and gyroscope measurements to obtain position and velocity and attitude then results in large accumulated errors. As a result, the IMU is usually augmented with other sensors to provide state feedback.

Despite its poor quality, the IMU does provide information on both the translational and rotational motion of the vehicle, allowing the potential for position and attitude to be determined. Errors in the sensors may be characterised using a strapdown inertial navigation system (SDINS), given accurate feedback from

other sources [5]. Assuming that these errors could be estimated during GNSS-aided flight, they could then be incorporated in the SDINS during periods of GNSS occlusion, improving state estimates.

As an alternative to the pure SDINS approach, knowledge of the system could be included in the Kalman filter algorithm. This has been shown to improve state estimates in large fixed-wing aircraft [6]. In including the quadrotor dynamics in the Kalman filter's system model, it may be possible to further improve position and attitude estimates. The aircraft may then be able to continue following the optimal flight path despite both the lack of additional on-board sensors and the intermittent and potentially prolonged loss of GNSS feedback. This paper therefore investigates the improvements in state estimation when using a good dynamic model of the quadrotor, as applied in simulation.

2 Qball-X4 MAV

2.1 Vehicle Platform

The simulation uses empirical data from flight tests of the Qball-X4 quadrotor MAV[1] (Figure 2). The Qball follows the convention of the quadrotor platform, with all control and propulsion achieved through the four 10-inch propellers spaced equally around the centre of gravity. Vehicle control is provided by adjustment of the speed, and therefore thrust and torque, of each rotor via pulse-width modulation (PWM) of the power

---

[1] http://www.quanser.com

Table 1 Qball system properties.

Parameter	Symbol	Value
Mass	m	1.54 kg
Moment of inertia about x	I_x	0.03 kg/m^2
Moment of inertia about y	I_y	0.03 kg/m^2
Moment of inertia about z	I_z	0.04 kg/m^2
Drag coefficient	c_d	0.1
Rotor distance from CG	L	0.2 m
Rotor thrust ratio	K_T	120 N
Rotor torque ratio	K_Q	4 N m
Thrust time constant	τ_T	0.0667 s
Torque time constant	τ_Q	0.0667 s

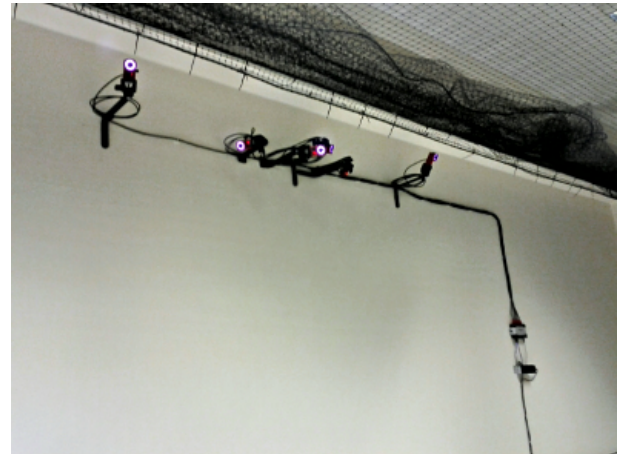**Fig. 3** Camera cluster in Optitrack motion capture system.

input. Housed at the centre of gravity of the Qball is a Gumstix embedded computer, HiQ data acquisition card (DAQ) and IMU. The HiQ DAQ receives data from each of the sensors and provides commands for each propeller motor to the electronic speed controller (ESC). The vehicle systems communicate with a ground-station PC via wi-fi, allowing high-speed, two-way transfer of data. A sonar sensor is mounted on the bottom of the vehicle for height measurements.

The IMU contains accelerometers, gyroscopes and magnetometers, each providing three-axis measurements in the vehicle body frame. For the purposes of the experiment, the magnetometer measurements are ignored, as they are strongly affected by electrical equipment such as that in the flight lab. The sonar measurements are also neglected, to focus only on IMU performance.

2.2 Operating Environment

A flight testing laboratory is available for experimental testing of micro air vehicles, allowing flights to take place in a safe, controlled environment. However, in restricting flights of the Qball to indoors, the use of GNSS is precluded entirely. As an alternative, the Optitrack motion capture system[2] is used to provide both position and attitude feedback to the Qball (Figure 3). The Optitrack system delivers far greater accuracy in its measurements than GNSS, but nevertheless allows the scenario discussed in the introduction to be replicated to a degree.

The system uses a group of infrared cameras arranged around the desired flight volume. Ensuring that an object in the flight space is visible from at least 3 cameras, the calibrated system is able to determine the position of the object in a chosen axes system. A single reflective market is be used for position tracking. For attitude tracking and position tracking of multiple objects, it is possible to define asymmetric, unique groups of markers as rigid bodies.

Thus, for the purposes of the simulation, it is assumed both position and attitude feedback are available from the Optitrack system. This provides the information on both the linear and angular motion of the vehicle required to characterise the sensor errors. In outdoor flights, alternatives could be explored to provide accurate attitude estimates, including sensor fusion and complementary filtering [7].
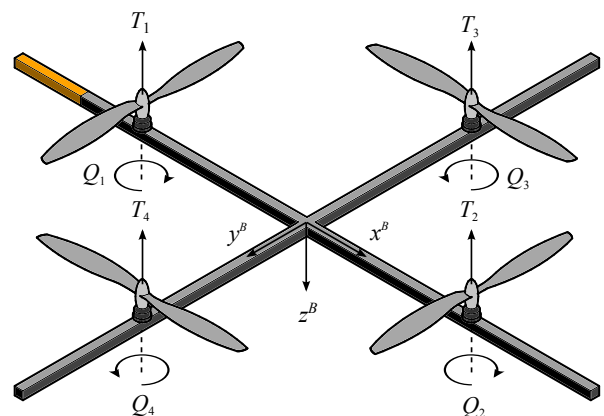
Fig. 4 Qball rotor positions and numbering

---

[2]http://www.naturalpoint.com

2.3 Quadrotor Model

Quadrotor dynamics are well-covered in literature [5, 8, 9, 10], but may be summarised as

$$\dot{\mathbf{r}} = \mathbf{R}_B^E \mathbf{v} \tag{1}$$

$$\dot{\mathbf{v}} = \frac{1}{m}\mathbf{F} - \boldsymbol{\omega} \times \mathbf{v} \tag{2}$$

$$\dot{\boldsymbol{\eta}} = \mathbf{J}\boldsymbol{\omega} \tag{3}$$

$$\dot{\boldsymbol{\omega}} = \mathbf{I}^{-1}\left(\mathbf{M} - \boldsymbol{\omega} \times \mathbf{I}\boldsymbol{\omega}\right) \tag{4}$$

where (1) and (4) describe the kinematics of the system in the Earth-fixed frame; (2) describes the linear motion response to an input force, described in the vehicle body-fixed frame; and (4) describes the angular motion response to moment, also described in the body-fixed frame. The rotation matrices $\mathbf{R}_B^E$ and $\mathbf{J}$ are the transformation from one frame to another. The transformation from the body-fixed frame to the Earth-fixed frame is

$$\mathbf{R}_B^E = \begin{bmatrix} c_\theta c_\psi & -c_\phi s_\psi + s_\phi s_\theta c_\psi & s_\phi s_\psi + c_\phi s_\theta c_\psi \\ c_\theta s_\psi & c_\phi c_\psi + s_\phi s_\theta s_\psi & -s_\phi c_\psi + c_\phi s_\theta s_\psi \\ -s_\theta & s_\phi c_\theta & c_\phi c_\theta \end{bmatrix} \tag{5}$$

where c_ϕ denotes $\cos\phi$, s_θ is $\sin\theta$, etc. The transformation from angular body rates to rate of change of Euler angles is

$$\mathbf{J} = \begin{bmatrix} 1 & \sin\phi\tan\theta & \cos\phi\tan\theta \\ 0 & \cos\phi & -\sin\phi \\ 0 & \sin\phi\sec\theta & \cos\phi\sec\theta \end{bmatrix} \tag{6}$$

Each rotor i produces a thrust and torque which is proportional to the input signal u, with dynamics modelled by a first-order lag:

$$\dot{T_i} = -\frac{1}{\tau_T}T_i + \frac{1}{\tau_T}K_T u_i \tag{7}$$

$$\dot{Q_i} = -\frac{1}{\tau_Q}Q_i + \frac{1}{\tau_Q}K_Q u_i \tag{8}$$

The force vector $\mathbf{F}$ is then the sum of the inertial, propulsive and aerodynamic forces acting upon the vehicle:

$$\mathbf{F} = m\mathbf{R}_E^B \begin{bmatrix} 0 \\ 0 \\ g \end{bmatrix} + \begin{bmatrix} 0 \\ 0 \\ -T_c \end{bmatrix} - c_d\mathbf{v} \tag{9}$$

where $\mathbf{R}_E^B$ is the transformation from the Earth-fixed frame to the body-fixed frame and is given by the transpose of the reverse transformation $\mathbf{R}_E^B = \mathbf{R}_B^{E^T}$. The collective thrust T_c is

$$T_c = T_1 + T_2 + T_3 + T_4 \tag{10}$$
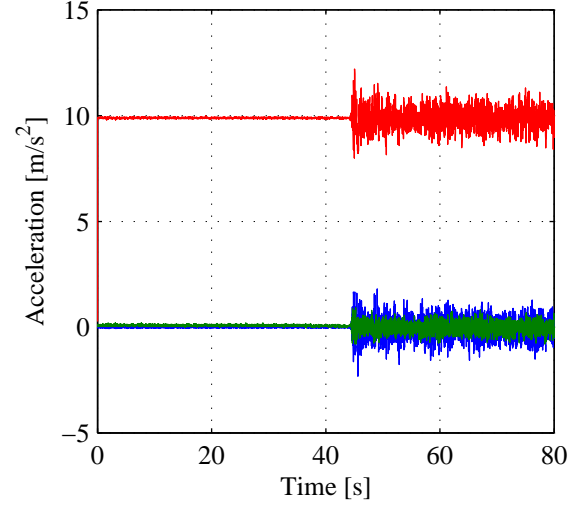
Fig. 5 Accelerometer output during experimental test flight. The propellers are inactive until $t \approx 45s$, when the effect of frame vibration becomes apparent.

The moment vector $\mathbf{M}$ is formed from the thrust and torque differentials produced by the rotors:

$$\mathbf{M} = \begin{bmatrix} L(T_3 - T_4) \\ L(T_2 - T_1) \\ -Q_1 - Q_2 + Q_3 + Q_4 \end{bmatrix} \tag{11}$$

where the rotors are positioned as in Figure 4.

2.4 Sensor Model

MEMS sensors such as those found on the Qball are subject to a variety of errors in their measurements. For flight durations of several minutes, the most prominent errors in both the accelerometers and gyroscopes are a constant bias and a thermo-mechanical white noise [5]. The accelerometer outputs may then be modelled as the sum of the specific force acting on the quadrotor, a constant bias and a zero-mean Gaussian white noise

$$\hat{\mathbf{a}} = \mathbf{a}_p + \mathbf{b}_a + \mathbf{w}_a \tag{12}$$

where the specific force, or proper acceleration, $\mathbf{a}_p$ is the non-gravitational acceleration acting upon the vehicle.

Similarly, the gyroscope is modelled as the sum of the angular body rates of the vehicle, a bias and white noise

$$\hat{\mathbf{g}} = \boldsymbol{\omega} + \mathbf{b}_g + \mathbf{w}_g \tag{13}$$

The biases are dependent on a number of factors, including temperature, and change from flight

Table 2 Biases in sensor measurements

Sensor	Error range
Accelerometer	± 0.15 m/s^2
Gyroscope	± 0.01 rad/s

Table 3 Standard deviations in measurement noises

Sensor	Standard deviation	
	No Vibration	With Vibration
Accelerometer	0.022 m/s^2	0.443 m/s^2
Gyroscope	0.003 rad/s	0.009 rad/s

to flight. The sensor noises are accounted for in the Kalman filter algorithm described in Section 3. Tables 2 and 3 describe the bias and noise attributes of the sensors, acquired through experimental testing. Note that there is a significant increase in the apparent noise of the accelerometer (and to a lesser extent, the gyroscope) measurements after a short time (Figure 5). This is due to vibration of the vehicle frame when the propellers are operating. This may be considered a process noise in the vehicle dynamics which is measured by the accelerometers and gyroscopes. Without knowing how the vibration influences the dynamics of the vehicle, it is included in the simulation model as an increase in accelerometer and gyroscope noise.

3 Navigation Algorithms

A standard SDINS is employed in estimating the biases while the Optitrack system is providing position and attitude feedback. Upon losing this data, two alternatives are explored:

1. Continued use of the SDINS, using the bias estimates to obtain accurate state estimates from the accelerometers and gyroscopes.

2. Use of a dynamic model of the quadrotor to provide superior prediction of states, and including the bias estimates to obtain accurate measurements from sensors.

Each of these algorithms is implemented using the extended Kalman filter (EKF), a variation of the Kalman filter designed for non-linear systems. The EKF is designed to estimate the states of a non-linear

system of the form

$$\dot{\mathbf{x}}(t) = f(\mathbf{x}(t), \mathbf{u}(t), \mathbf{w}_p(t)) \tag{14}$$

$$\mathbf{y}(t) = h(\mathbf{x}(t), \mathbf{u}(t), \mathbf{w}_m(t)) \tag{15}$$

where (14) describes the process model of the system and (15) describes the measurement model.

The EKF, as described by Welch and Bishop [11], estimates the state $\mathbf{x}$ of a system by modelling the system processes and measurements and attempting to minimise the errors in any estimates through comparison with real measurement data. The algorithm may be considered as two distinct parts. The prediction step estimates the current system state and error covariance using a model of the system, the previous state and error covariance and the real system input:

$$\hat{\mathbf{x}}_{k|k-1} = f(\hat{\mathbf{x}}_{k-1|k-1}, \mathbf{u}_{k-1}) \tag{16a}$$

$$\mathbf{P}_{k|k-1} = \mathbf{A}_{k-1}\mathbf{P}_{k-1|k-1}\mathbf{A}_{k-1}^T + \mathbf{Q} \tag{16b}$$

The update step then uses this *a priori* estimate to produce an *a posteriori* estimate by incorporating the measurement model and the system outputs:

$$\mathbf{K}_k = \mathbf{P}_{k|k-1}\mathbf{C}_k^T \left(\mathbf{C}_k\mathbf{P}_{k|k-1}\mathbf{C}_k^T + \mathbf{R} \right)^{-1} \tag{16c}$$

$$\hat{\mathbf{x}}_{k|k} = \hat{\mathbf{x}}_{k|k-1} + \mathbf{K}_k \left(\mathbf{y}_k - h(\hat{\mathbf{x}}_{k|k-1}, \mathbf{u}_{k-1}) \right) \tag{16d}$$

$$\mathbf{P}_{k|k} = (\mathbf{I}_d - \mathbf{K}_k\mathbf{C}_k)\,\mathbf{P}_{k|k-1} \tag{16e}$$

The EKF equations are described in discrete time, where $\hat{\mathbf{x}}_{n|m}$ represents the state estimate at step n, given observations up to, and including, those at step m. This applies similarly to the error covariance matrix $\mathbf{P}_{n|m}$. The result of the algorithm is then the state estimate $\hat{\mathbf{x}}$ at step k, or time t_k. The state transition $\mathbf{A}$ and observation $\mathbf{C}$ matrices are defined as the Jacobians of the process and measurement models with respect to the state:

$$\mathbf{A}_{k-1} = \frac{\partial f}{\partial \mathbf{x}}\bigg|_{\hat{\mathbf{x}}_{k-1|k-1}, \mathbf{u}_{k-1}} \tag{17}$$

$$\mathbf{C}_k = \frac{\partial h}{\partial \mathbf{x}}\bigg|_{\hat{\mathbf{x}}_{k|k-1}, \mathbf{u}_{k-1}} \tag{18}$$

The Jacobians are determined analytically and implemented in the Kalman filter algorithm as algebraic expressions. This reduces the need to calculate the partial derivatives numerically with each iteration and allows the filter to run in real-time.

As stated, the EKF requires models of both the system process and sensors to predict and then update the state estimates. The more accurate the model, the

smaller the measurement residual and the superior the estimates. The models employed by the EKF for state estimation of the Qball quadrotor MAV are described in this section. First, the SDINS algorithm used to estimate the sensor biases, given accurate position and attitude measurements, is described. Next, a variation on this model is presented, neglecting the Optitrack measurements and attempting to predict the state transition with no knowledge of the vehicle dynamics. This solution uses the previous bias estimates to obtain more accurate measurements from the sensors. Finally, vehicle dynamics are included to provide a superior estimate in the absence of accurate state observations from the sensors. Again, this uses the sensor bias estimates to improve the measurement accuracy.

The models are described here in continuous time in the form

$$\dot{\mathbf{x}}(t) = f(\mathbf{x}(t), \mathbf{u}(t)) \tag{19}$$

$$\mathbf{y}(t) = h(\mathbf{x}(t), \mathbf{u}(t)) \tag{20}$$

then transformed to discrete time using forward differencing and implemented in the simulation.

3.1   Bias Estimation Using SDINS

Consider the sensor models described by (12) and (13). The accelerometers directly measure the specific force of the vehicle and therefore all of the non-inertial forces acting on it. This has the advantage of including all of the dynamics specific to the quadrotor without explicitly stating them. This applies similarly to the gyroscopes, which measure the angular rates of the aircraft. This method requires the accelerometer and gyroscope measurements to be supplied to the Kalman filter as inputs

$$\mathbf{u} = [\hat{a}_x, \hat{a}_y, \hat{a}_z, \hat{g}_x, \hat{g}_y, \hat{g}_z]^T \tag{21}$$

Then, using the sensors models given previously, the response of the vehicle may be described in terms of the body kinematics, sensor measurements and biases. Thus, with the state vector

$$\mathbf{x} = [x, y, z, u, v, w, \phi, \theta, \psi, \ldots$$
$$\ldots b_{ax}, b_{ay}, b_{az}, b_{gx}, b_{gy}, b_{gz}]^T \tag{22}$$

the SDINS model is

$$\dot{\mathbf{r}} = \mathbf{R}_B^E \mathbf{v} \tag{23a}$$

$$\dot{\mathbf{v}} = \hat{\mathbf{a}} - \mathbf{b}_a + \mathbf{R}_E^B \begin{bmatrix} 0 \\ 0 \\ g \end{bmatrix} - (\hat{\mathbf{g}} - \mathbf{b}_g) \times \mathbf{v} \tag{23b}$$

$$\dot{\boldsymbol{\eta}} = \mathbf{J}(\hat{\mathbf{g}} - \mathbf{b}_g) \tag{23c}$$

$$\dot{\mathbf{b}}_a = \mathbf{0} \tag{23d}$$

$$\dot{\mathbf{b}}_g = \mathbf{0} \tag{23e}$$

The Optitrack system provides accurate position and attitude feedback, thus for the measurement vector

$$\mathbf{y} = [\hat{o}_x, \hat{o}_y, \hat{o}_z, \hat{o}_\phi, \hat{o}_\theta, \hat{o}_\psi]^T \tag{24}$$

the sensor model is simply

$$\begin{bmatrix} \hat{o}_x \\ \hat{o}_y \\ \hat{o}_z \\ \hat{o}_\phi \\ \hat{o}_\theta \\ \hat{o}_\psi \end{bmatrix} = \begin{bmatrix} x \\ y \\ z \\ \phi \\ \theta \\ \psi \end{bmatrix} \tag{25}$$

This system is observable due to the feedback from the Optitrack system. In addition to estimating the position, velocity and attitude of the quadrotor, this solution is able to estimate the constant bias errors from each of the sensors.

3.2   Position, Velocity and Attitude Estimation Using SDINS

For instances where the Optitrack signal is lost, akin to periods of GNSS outage, the SDINS algorithm may continue to provide state estimates using the previous estimates of both state and error covariance. The lack of Optitrack feedback and the use of accelerometer and gyroscope measurements as model inputs results in the system being unobservable. Without any observations to correct the *a priori* estimate, the EKF uses the prediction step only.

The input and state vectors are therefore identical to those described in Section 3.1 and given by (21) and (22). Similarly, the process model is given by Equations (23a) to (23e). The accelerometer and gyroscope measurements are supplied to the algorithm as inputs, hence there is no measurement vector and thus no measurement model is required. Since the bias estimates using this method are held constant from the

final estimate obtained with Optitrack feedback, the accuracy of this solution is strongly dependent on estimating the biases accurately.

3.3 Position, Velocity and Attitude Estimation Using a Model-Augmented INS

In place of the kinematic solution used in the SDINS, a model incorporating the dynamics of the quadrotor is implemented. Considering a simplified version of the system model described in Section 2.3, the inputs to the EKF model are the PWM signals to the propeller motors

$$\mathbf{u} = [u_1, u_2, u_3, u_4]^T \tag{26}$$

and the states are expanded to include the angular body rates

$$\mathbf{x} = [x, y, z, u, v, w, \phi, \theta, \psi, p, q, r, \dots$$
$$\dots b_{ax}, b_{ay}, b_{az}, b_{gx}, b_{gy}, b_{gz}]^T \tag{27}$$

The process model includes the contribution of the airframe drag and propeller thrusts and torques to the motion of the aircraft, neglecting the dynamics in the propeller model:

$$\dot{\mathbf{r}} = \mathbf{R}_B^E \mathbf{v} \tag{28a}$$

$$\dot{\mathbf{v}} = \frac{1}{m} \left(\begin{bmatrix} 0 \\ 0 \\ -K_T(u_1 + u_2 + u_3 + u_4) \end{bmatrix} - c_d \mathbf{v} \right)$$
$$+ \mathbf{R}_E^B \begin{bmatrix} 0 \\ 0 \\ g \end{bmatrix} - \boldsymbol{\omega} \times \mathbf{v} \tag{28b}$$

$$\dot{\boldsymbol{\eta}} = \mathbf{J}\boldsymbol{\omega} \tag{28c}$$

$$\dot{\boldsymbol{\omega}} = \mathbf{I}^{-1} \left(\begin{bmatrix} LK_T(u_3 - u_4) \\ LK_T(u_2 - u_1) \\ K_Q(-u_1 - u_2 + u_3 + u_4) \end{bmatrix} \right.$$
$$\left. - \boldsymbol{\omega} \times \mathbf{I}\boldsymbol{\omega} \right) \tag{28d}$$

$$\dot{\mathbf{b}}_a = \mathbf{0} \tag{28e}$$

$$\dot{\mathbf{b}}_g = \mathbf{0} \tag{28f}$$

In this case, the accelerometer and gyroscope outputs are included in the measurement vector, making the system observable:

$$\mathbf{y} = [\hat{a}_x, \hat{a}_y, \hat{a}_z, \hat{g}_x, \hat{g}_y, \hat{g}_z]^T \tag{29}$$

and the measurement model uses the known dynamics

of the vehicle to predict the sensor outputs

$$\hat{\mathbf{a}} = \frac{1}{m} \left(\begin{bmatrix} 0 \\ 0 \\ -K_T(u_1 + u_2 + u_3 + u_4) \end{bmatrix} - c_d \mathbf{v} \right)$$
$$+ \mathbf{b}_a \tag{30a}$$

$$\hat{\mathbf{g}} = \boldsymbol{\omega} + \mathbf{b}_g \tag{30b}$$

4 Simulation Results

Three variations of the simulation were run. The first neglects the process and measurement noise in the system, thus the only errors in the accelerometer and gyroscope measurements are the biases. The second includes a small amount of process noise and measurement noise based on experimental data from flights of the Qball and detailed in Table 3. The third variation includes the increased apparent noise in the accelerometer measurements due to vibration from the propellers. This vibration represents a process rather than measurement noise, but is included in the sensor model due to lack of information on its actual effect on the dynamics of the system.

The simulation was run using a 4th-order Runge-Kutta solver with a time increment of 0.005 s and the Kalman filters used an increment of 0.05 s. The runtime is 80 s, with Optitrack loss occurring 40 s after the simulation begins. The quadrotor begins at rest and then pursues a figure-of-eight path which is designed to simulate the constant motion and perturbation of the states that would occur in a practical flight. Initial simulation bias values were chosen based on the data given in Table 2 and were kept consistent across each iteration of the simulation.

4.1 Results with No Noise

Figure 6 demonstrates the results of each navigation algorithm when there is no process or measurement noise in the system. With external feedback available, the accelerometer and gyroscope bias estimates quickly converge on the simulation values. Thus, when the external feedback is lost, the SDINS algorithm is able to provide accurate estimates of position, velocity and attitude for a short period of time, despite the lack of observability in the model. The model-augmented INS is shown to provide similarly accurate state estimates for the noiseless system. The minimal error in both solutions arises from the difference in time increment between the Kalman filter and simulation, and the small error in the bias estimation.
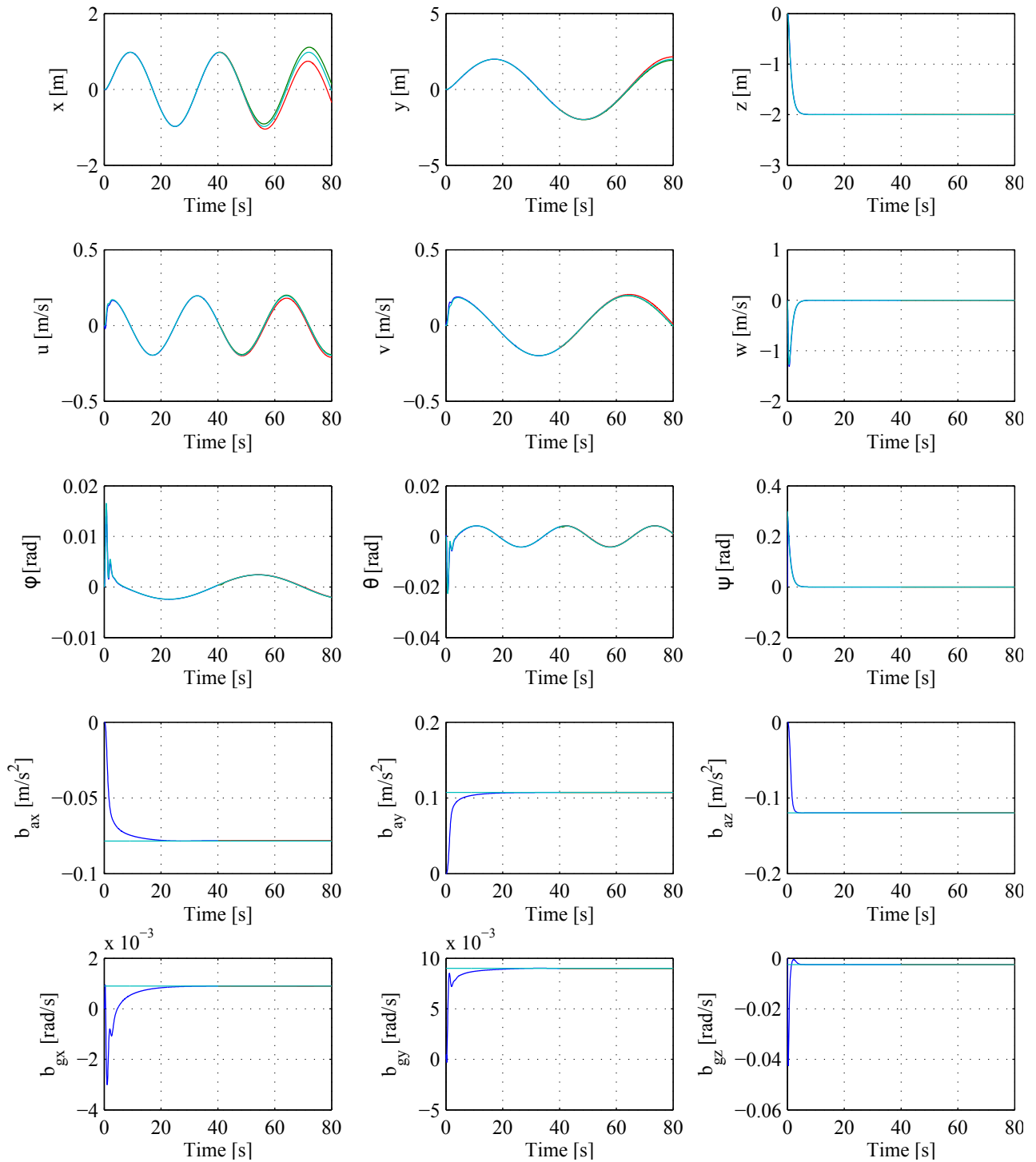
Fig. 6 State estimation of noiseless system. Simulation states - cyan; SDINS state estimation with Optitrack feedback – blue; SDINS state estimation without Optitrack – red; state estimation without Optitrack using model-augmented INS – green.

4.2 Results with Noise from Experimental Tests

Figure 7 shows the results when there is non-zero noise in both the process and measurement models. The noise in the system now results in a less accurate estimate of the sensor biases, causing the SDINS state estimates to quickly diverge from the true values (Figure 8). With the improved observability of the model-augmented INS, the residual in the state estimates is much lower, although still larger than desired for flight in constrained environments (Figure 9). With the inclusion of process noise, the sensor biases now experience a random walk and deviate slightly from the initial values. This is consistent with sensor models described by Wierema [5] and used in the simulation.

4.3 Results with Noise and Vehicle Vibration

Figure 10 shows the results of the simulation when both system noise and vibration interference are included. Although the vibration affects the dynamic response of the system itself, it is restricted to sensor interference in this instance. The increased error in the sensor feedback results in a poorer estimate of the biases, causing a greater drift in the integrated state estimates. While the error is much smaller in the model-augmented INS, it is still significant.

5 Conclusions

The simulation results demonstrate that a sufficiently accurate model of a system is able to improve the estimates of the extended Kalman filter algorithm and enable the quadrotor to continue along the optimal path. Figures 8 and 9 show that the difference in the position and attitude residuals of each method is significant, with the SDINS errors quickly diverging. The errors in the model-augmented INS are small enough that the quadrotor would be able to continue operating in an urban canyon of sufficiently great size, such as a street or large room, for approximately as long as a minute after external feedback loss.

Including the effect of vehicle vibration of the sensor measurements, the model-augmented INS is again superior to the SDINS in its state estimates. However, the increased apparent noise in the measurements results in much greater errors in the estimates of both solutions. The position and attitude residuals in the model-augmented INS are significant enough to render it unusable in a practical capacity.

Experimental testing of the model-augmented

INS requires that the vibration issue is resolved before any navigation algorithm is implemented on the Qball. Since the operation of the propellers is the source of the vibration, it may be possible to determine a vibration model for the Qball and include it in both the simulation model and the Kalman filter algorithm. Alternatively, a physical solution may be explored, such as placement of dampers between the rotor mounts and vehicle frame.

Neglecting the detrimental effects of the vibration, any experimental testing may require a superior model of the system. While the model employed in the navigation solution is sufficiently accurate in comparison to the simulation's system model, it may not be representative of the true quadrotor dynamic processes. Therefore, in continuing this research, two issues will have to be resolved: the vehicle vibration; and the development of an accurate system model. This second aim will be investigated through the design and implementation of a multi-fidelity model of the quadrotor, with successively higher fidelity models constructed until the system dynamics are accurately represented.

References

[1] J. Hall and D. Anderson, "Reactive route selection from pre-calculated trajectories – application to micro-UAV path planning," *The Aeronautical Journal*, vol. 115, no. 1172, pp. 635–640, 2011.

[2] R. He, S. Prentice, and N. Roy, "Planning in Information Space for a Quadrotor Helicopter in a GPS-denied Environment," in *2008 IEEE International Conference on Robotics and Automation*. Pasadena, CA: IEEE, May 2008, pp. 1814–1820.

[3] C. Kemp, "Visual Control of a Miniature Quad-Rotor Helicopter," PhD, University of Cambridge, 2006.

[4] J. Kim and S. Sukkarieh, "SLAM aided GPS/INS navigation in GPS denied and unknown environments," in *2004 International Symposium on GNSS/GPS*, no. December, 2004.

[5] M. Wierema, "Design, implementation and flight test of indoor navigation and control system for a quadrotor UAV," Masters Thesis, Delft University of Technology, 2008.
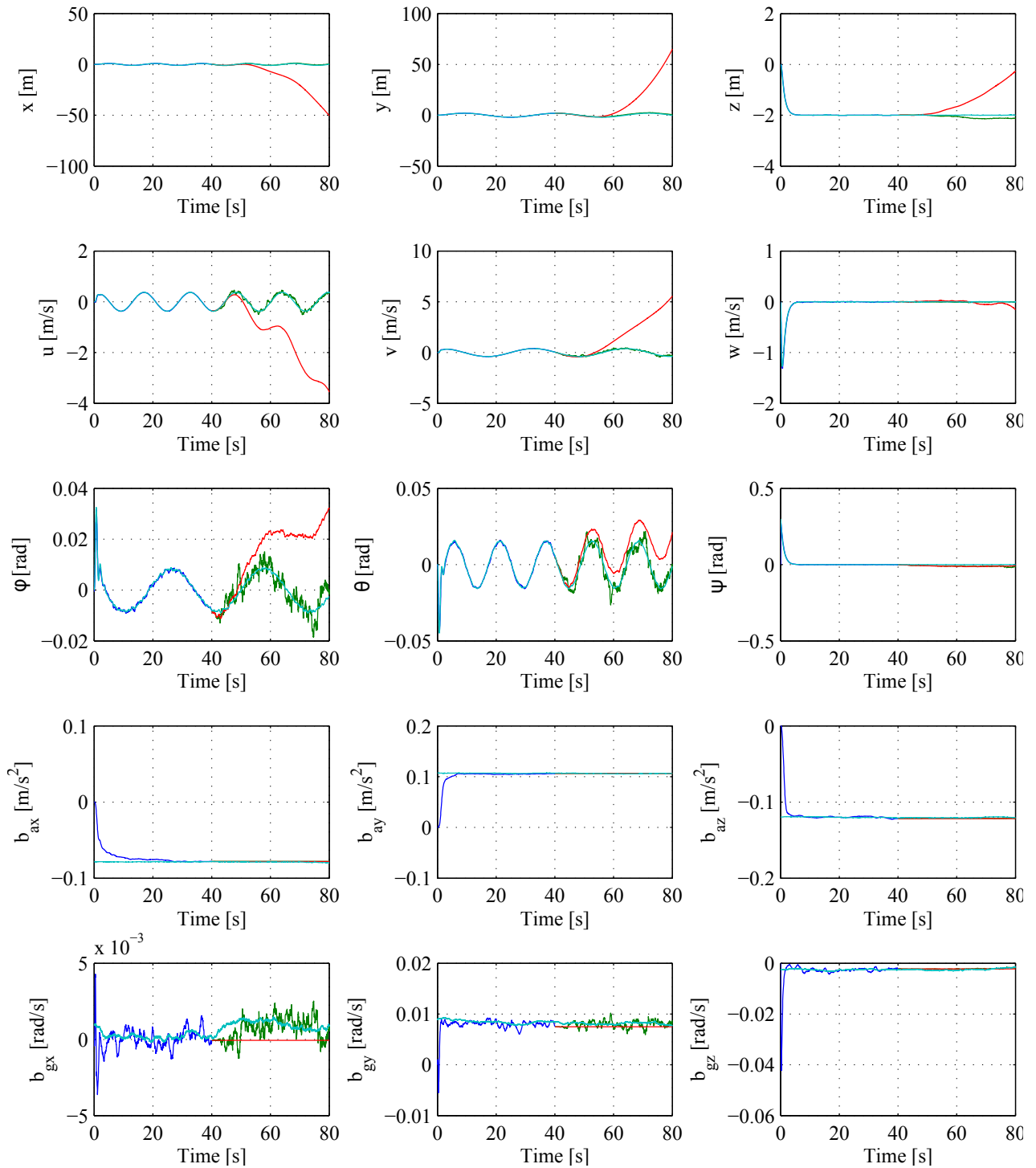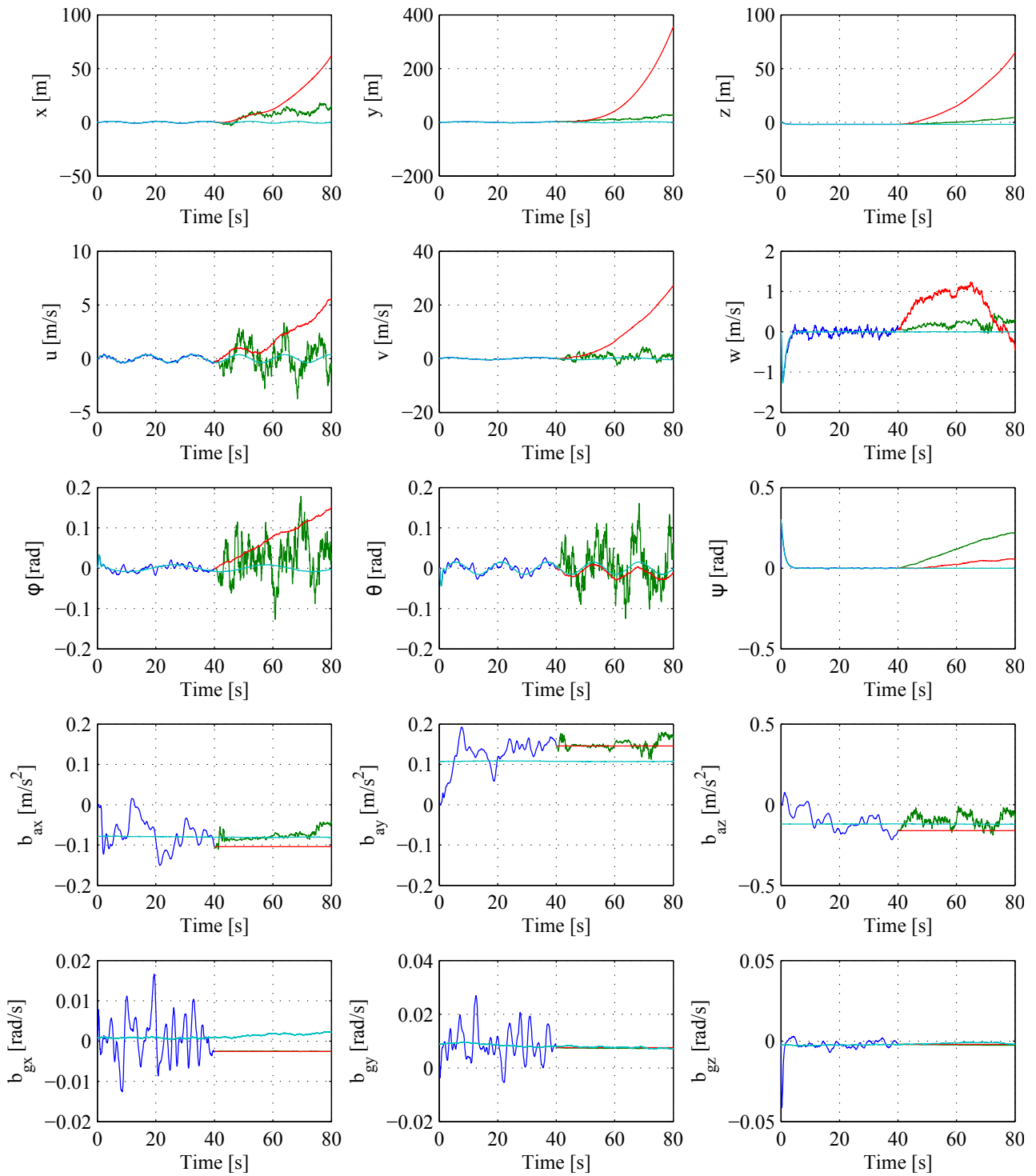
Fig. 7 State Estimation of system with realistic noise. Simulation states - cyan; SDINS state estimation with Optitrack feedback – blue; SDINS state estimation without Optitrack – red; state estimation without Optitrack using model-augmented INS – green.
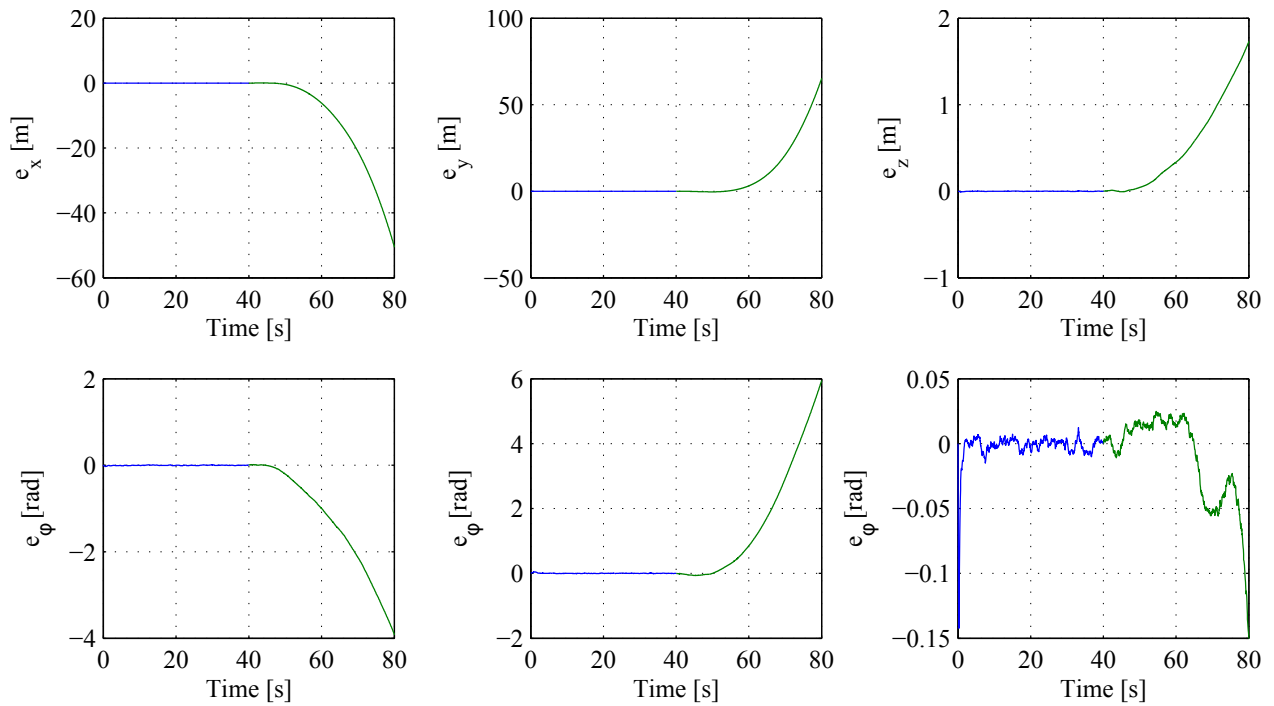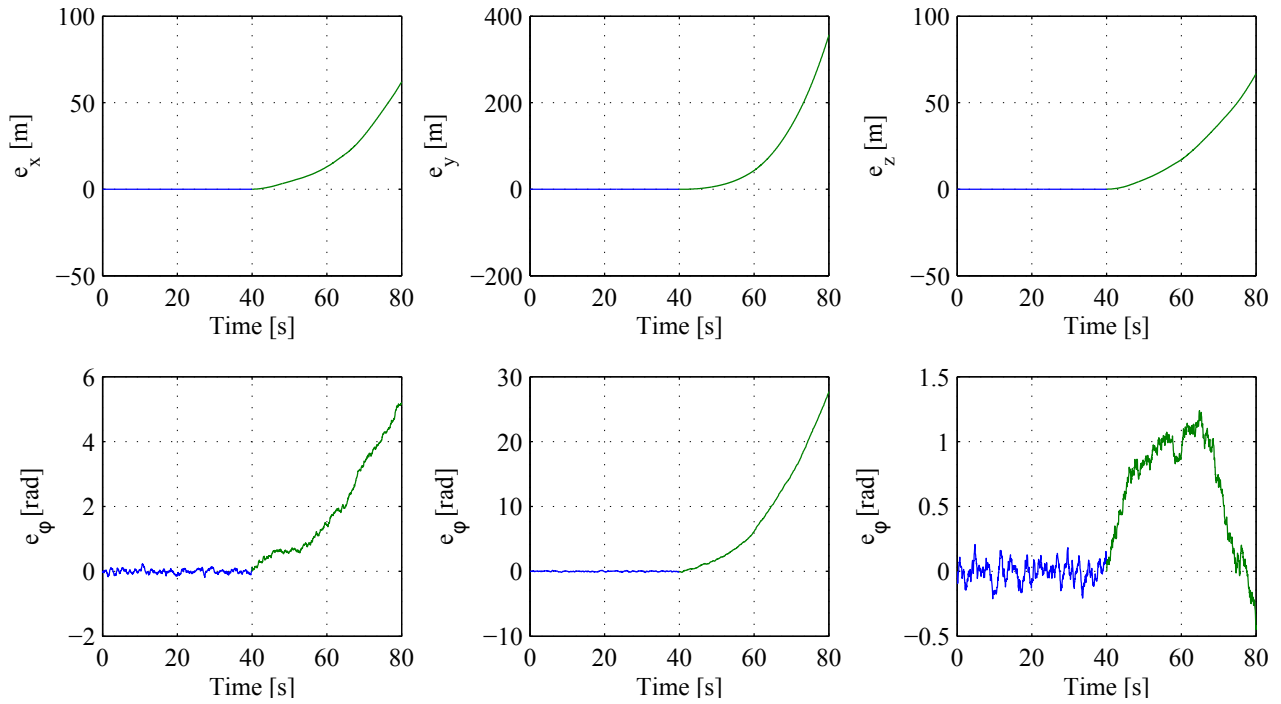
Fig. 8 Position and attitude errors in system with realistic noise, using SDINS to estimate states. Optitrack feedback available – blue; Optitrack feedback unavailable – green.
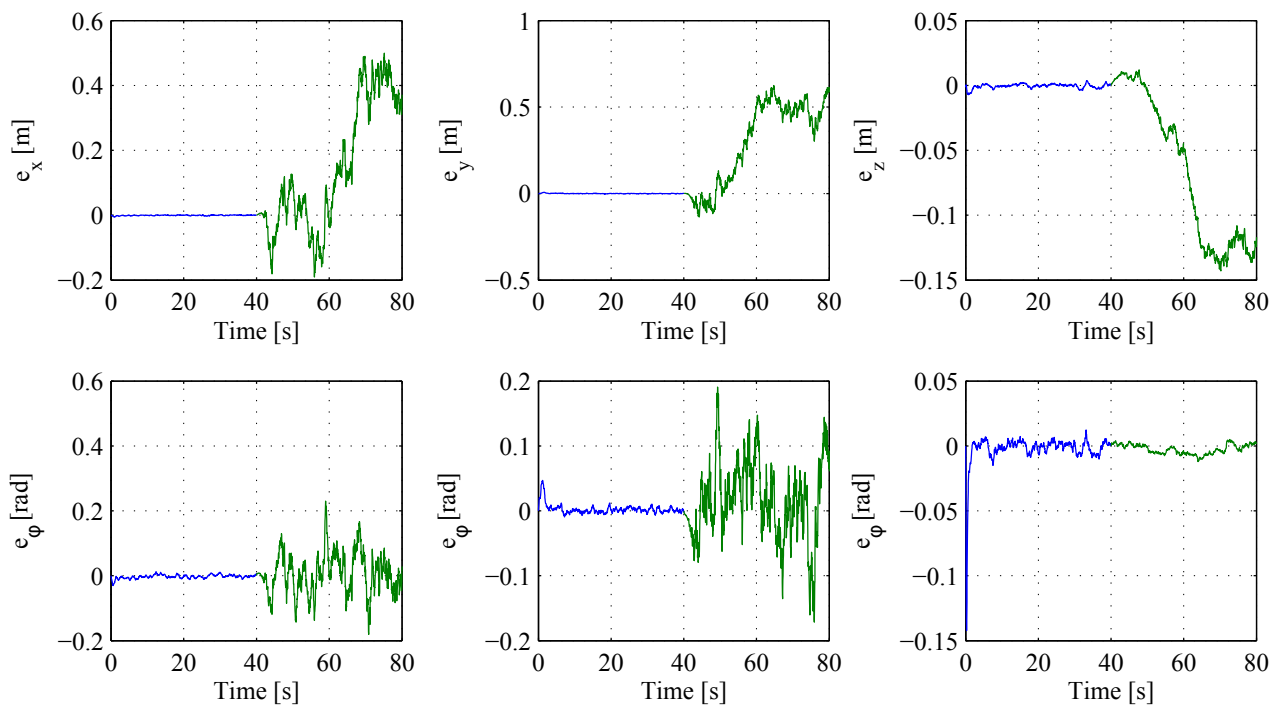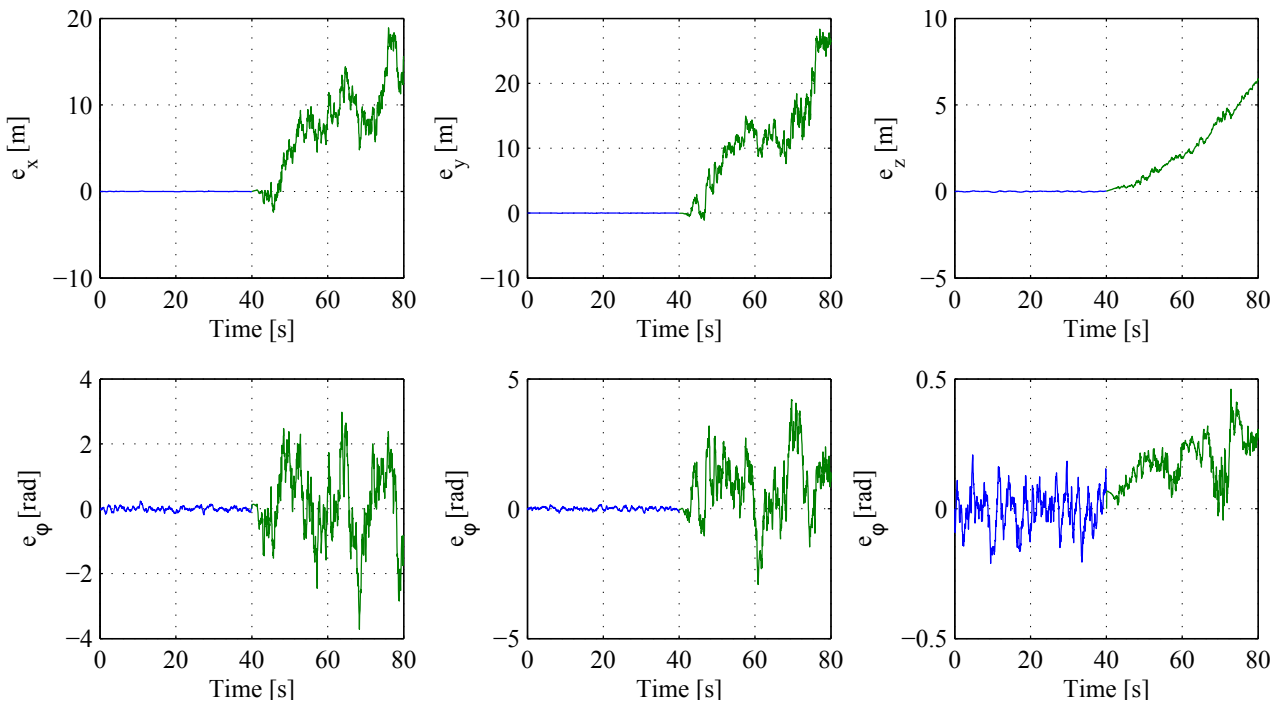

Fig. 9 Position and attitude errors in system with realistic noise, using model-augmented INS to estimate states without external state feedback. Optitrack feedback available – blue; Optitrack feedback unavailable – green.

Fig. 10 State Estimation of system with realistic noise and vibration interference. Simulation states - cyan; SDINS state estimation with Optitrack feedback – blue; SDINS state estimation without Optitrack – red; state estimation without Optitrack using model-augmented INS – green.

Fig. 11 Position and attitude errors in system with realistic noise and vibration interference, using SDINS to estimate states. Optitrack feedback available – blue; Optitrack feedback unavailable – green.

Fig. 12 Position and attitude errors in system with realistic noise and vibration interference, using model-augmented INS to estimate states without external state feedback. Optitrack feedback available – blue; Optitrack feedback unavailable – green.

[6] M. Koifman and I. Bar-Itzhack, "Inertial Navigation System Aided by Aircraft Dynamics," *IEEE Transactions on Control Systems Technology*, vol. 7, no. 4, pp. 487–493, Jul. 1999.

[7] W. Higgins, "A Comparison of Complementary and Kalman Filtering," *IEEE Transactions on Aerospace and Electronic Systems*, vol. AES-11, no. 3, pp. 321–325, May 1975.

[8] R. W. Beard, "Quadrotor Dynamics and Control," Brigham Young University, Provo, UT, Tech. Rep., 2008.

[9] S. Bouabdallah and R. Siegwart, "Design and Control of a Miniature Quadrotor," *Advances in Unmanned Aerial Vehicles*, 2007.

[10] C. Chamberlain, "System Identification, State Estimation, and Control of Unmanned Aerial Robots," MSc Thesis, Brigham Young University, 2011.

[11] G. Welch and G. Bishop, "An Introduction to the Kalman Filter," University of North Carolina at Chapel Hill, Chapel Hill, NC, Tech. Rep., 2006.

Nomenclature

This is how long this column should be and no longer

$\mathbf{A}$	State transition matrix
$\mathbf{a}_p$	Proper acceleration or specific force
$\hat{\mathbf{a}} = [\hat{a}_x, \hat{a}_y, \hat{a}_z]^T$	Accelerometer measurement
$\mathbf{b}_a = [b_{ax}, b_{ay}, b_{az}]^T$	Accelerometer bias vector
$\mathbf{b}_g = [b_{gx}, b_{gy}, b_{gz}]^T$	Gyroscope bias vector
$\mathbf{C}$	Observation matrix
c_d	Drag coefficient
$\mathbf{F}$	Force vector
f	State transition model
g	Acceleration due to gravity
$\hat{\mathbf{g}} = [\hat{g}_x, \hat{g}_y, \hat{g}_z]^T$	Gyroscope measurement
h	Measurement model
$\mathbf{I} = \begin{bmatrix} I_x & 0 & 0 \\ 0 & I_y & 0 \\ 0 & 0 & I_z \end{bmatrix}$	Inertia matrix
$\mathbf{I}_d$	Identity matrix
$\mathbf{J}$	Angular rate transformation matrix
K_Q	Torque-to-input gain
K_T	Thrust-to-input gain
$\mathbf{K}$	Kalman gain
L	Propeller distance from CG
$\mathbf{M}$	Moment vector
m	Mass
$\hat{\mathbf{o}} = [\hat{o}_x, \hat{o}_y, \hat{o}_z, \dots \dots \hat{o}_\phi, \hat{o}_\theta, \hat{o}_\psi]^T$	Optitrack measurements
$\mathbf{P}$	Error covariance matrix
Q	Torque
$\mathbf{Q}$	Process noise covariance
$\mathbf{R}$	Measurement noise covariance
$\mathbf{R}_B^E$	Direction cosine matrix for body-to-Earth transformation
$\mathbf{r} = [x, y, z]^T$	Position in Earth-fixed frame
T	Thrust
u	Propeller motor input
$\mathbf{u}$	Input vector
$\mathbf{v} = [u, v, w]^T$	Velocity in body-fixed frame
$\mathbf{w}_a$	Accelerometer noise
$\mathbf{w}_g$	Gyroscope noise
$\mathbf{w}_m$	Measurement noise
$\mathbf{w}_p$	Process noise
$\mathbf{x}$	System state vector
$\mathbf{y}$	System measurement vector
$\boldsymbol{\eta} = [\phi, \theta, \psi]^T$	Attitude in Euler angles
τ_Q	Torque time constant
τ_T	Thrust time constant
$\boldsymbol{\omega} = [p, q, r]^T$	Body angular velocities

Copyright Statement